IUST
Iran University of Science and Technology

Iranian Journal of Electrical and Electronic Engineering

Journal Homepage: ijeee.iust.ac.ir

A High Voltage Gain DC-DC Converter Based on Quadratic Boost Converter Suitable for Renewable Energy Resources

S. Hasanzadeh*(C.A.), S. M. Salehi**, and M. J. Saadatmandfar*

Abstract: Various forms of distributed generation (DG), such as photovoltaic (PV) systems, play a crucial role in advancing a more sustainable future, driven by economic factors and environmental policies implemented by governments. DC-DC converters are essential for harnessing power from solar cells, as they maintain a constant output voltage despite fluctuations in input voltage. Typically, step-up converters are employed to raise output voltage levels, though they often apply the same voltage to an active switch as the output voltage, which can be limiting. To effectively integrate distributed generation sources with the utility grid, high-voltage gain step-up converters are necessary since these sources typically operate at low voltage levels. This study presents an enhanced design of non-isolated DC-DC converters with high voltage gain tailored for photovoltaic (PV) applications. The proposed architecture achieves a quadratic increase in output voltage gain, which alleviates voltage stress on the active switch. Our converter design features a quadratic boost converter complemented by a voltage-boosting cell, facilitating significant voltage amplification. This topology benefits from employing an active switch while minimizing the number of inductors required, resulting in a more compact circuit design. Furthermore, the proposed architecture shares characteristics with recently published topologies regarding passive component utilization, voltage gain, and other relevant parameters. To validate our findings, we conducted mathematical analyses and simulations, with results corroborated by experimental data from laboratory prototype tests.

Keywords: DC-DC Converter, High Voltage Gain, Quadratic Boost Converter, Renewable Energy Resources.

1 Introduction

RECENTLY, Given the escalating seriousness of global warming, different fields of study are exploring methods to reduce greenhouse gas emissions. The burning of fossil fuels is usually the main cause of greenhouse gas emissions worldwide. Right now, when it comes to cleaning and enhancing the environment, renewable energy is the most beneficial choice available globally. While nuclear energy has the potential to generate clean and renewable energy, the handling of radioactive waste during post-processing poses significant risks to the planet's ecology and can have enduring adverse effects on human culture. This situation is a direct result of the refusal to use this energy source [1]. Renewable energy sources, specifically solar energy, are a steadfast and dependable means of energy generation that may imminently supplant energy systems reliant on fossil fuels. Nevertheless, solar cells have a

Iranian Journal of Electrical & Electronic Engineering, YYYY.
Paper first received DD MONTH YYYY and accepted DD MONTH YYYY.
* The authors are with the Department of Electrical and Computer Engineering, Qom university of Technology, Qom, Iran.
E-mails: hasanzadeh@qut.ac.ir, Mohammadsaadat167@iran.ir.

** The author is with the Department of Electrical Engineering, Tarbiat Modares University, Tehran, Iran.
E-mail: sm.salehi3@gmail.com.

Corresponding Author: Saeed Hasanzadeh.

restricted capacity to generate voltage, which is rather low. This is a challenge as numerous electrical devices necessitate a greater voltage output, both in direct current (DC) and alternating current (AC) modes. To increase voltage and produce energy, solar cells can be connected in parallel or in series. Nevertheless, this increase in voltage is still insufficient. Consequently, due to the limitation of solar modules to produce a maximum of 48 V, it is imperative to utilize a power electronic DC-DC step-up converter to achieve the required output voltage [2]. There are many other boost converter topologies available, but traditional ones suffer from issues with low voltage gain and high voltage stress on the active switch. To overcome this constraint, a new type of converter has been created: A converter with a high voltage gain. The converter lowers the voltage stress on the active switch and exhibits a notable improvement in voltage gain [3]. There are two main types of high-voltage gain converters: isolated and non-isolated. Medium-power applications commonly employ non-isolated converters due to their economical nature and superior efficiency. Scientists have presented different arrangements, each possessing its own benefits and drawbacks [4]. Typically, converters that have a large voltage gain utilize switched inductors, multiplier circuits, and switched capacitors. A typical step-up DC-DC converter implements several modifications to achieve a substantial voltage increase. Switched inductors and switched capacitors are frequently employed for this objective. A circuit comprising seven diodes, five capacitors, and three inductors has been constructed to obtain significant voltage gain by using a switchable inductor and a switchable capacitor [5]. Nevertheless, a certain degree of power loss is unavoidable throughout the process of conversion. A novel configuration has been introduced in [6], which entails the creation of an altered boost converter and voltage multiplier. However, this converter's lack of shared ground between the input and output leads to an undesired capacitance due to the disparity in ground voltage levels on each side. Renewable energy systems have suggested a step-up converter with a high voltage gain for application [7]. This converter has several notable characteristics, including uninterrupted input current, minimal voltage strain on active switches, and a shared ground connection between the input and output. Nevertheless, there are also certain drawbacks associated with this converter. For example, there are two active switches, one of which is floating, despite the fact that the gate signal for both converters is identical. In order to achieve a significant voltage rise, a voltage multiplier and a coupled inductor are integrated in a novel two-stage step-up converter that has been introduced [8]. The primary goal of this converter is to minimize the converter's losses by utilizing the energy stored in the coupled inductor's leakage inductor and transferring it to the load. Further, there is less voltage stress on the active switches due to the sharing of the converter's input and output grounds. A more sophisticated DC-DC converter is proposed in [9], which uses a coupled inductor to produce a large voltage gain. A three-winding coupled inductor can increase the number of degrees of freedom by two thanks to the circuit-turn ratio. As a result, the output voltage range is expanded. In order to simplify the management of the output voltage and active switch, two capacitors connected in series and a clamp are employed. The converter features a straightforward control mechanism that allows for simultaneous operation of the active switches. Nevertheless, the converter's input and output ground are not connected, which is an undesirable property for the converter. The utilization of a DC-DC converter has been proposed for renewable energy applications that necessitate a substantial voltage boost. The converter utilizes two voltage multiplier cells and a three-winding coupled inductor to achieve a significant increase in voltage [10]. This enables the utilization of an active switch that exhibits minimal resistance when in the on-state state and has a narrow range of acceptable voltage levels, resulting in fewer losses during conduction. In addition, the diodes are maintained at a minimum voltage level to minimize the reverse recovery issue and enhance efficiency. The converter's input and output grounds are connected, and the utilization of two capacitors in series at the output minimizes variations in the output voltage. A functioning key streamlines the management and propulsion systems of the converter. To enhance the voltage amplification of a step-up converter, a recommended approach is to use a voltage multiplier as a secondary stage within an interleaved architecture. This entails the sequential connection of two voltage-amplification stages. The authors of references [11] and [12] propose a two-phase converter that consists of two phases. Each phase includes a two-winding coupled inductor and a voltage multiplier. The primary goal was to achieve a substantial voltage increase by utilizing the secondary coils within the voltage multiplier. An advantage of this converter is its shared ground between the input and output, which prevents the active switches from floating and maintains the uninterrupted flow of input current. Nevertheless, incorporating the interleave approach into the converter control system may increase its complexity because it necessitates the inclusion of a phase shift circuit. [13] proposes a topology that provides both a substantial voltage amplification and excellent efficiency. Moreover, it is feasible to attain a substantial increase in voltage without requiring the converter to function at a high duty cycle by only

increasing the turn ratio of the coupled inductor. This converter has several advantages, including a common reference point, a small number of components, and low voltage stress on the active switch. The article in [14] introduces a converter with a substantial increase in voltage and is specifically tailored for use in renewable energy applications. The converter demonstrates a very high voltage amplification as a result of the limited number of turns in the intercoupled inductor. Additionally, it ensures a consistent input current and provides a wide array of adjustable voltage amplifications. The coupled inductor comprises a winding with a step-down design (turn ratio less than 1) and another winding with a step-up configuration. This configuration not only increases the voltage but also enables more versatile voltage control. The input current demonstrates negligible distortion, leading to a reduction in both the volume and capacity of the input filter. Additionally, the converter includes a switched capacitor that has an incorporated passive clamp circuit for the active switch. This reduces the likelihood of voltage spikes. The converter has a common ground for both the input and output and its active switch remains linked. A quasi-source impedance converter is suggested in [15], featuring a grounded active switch. The mentioned converter utilizes an additional dynamic switch and a diode, as opposed to the conventional impedance pseudo-source converter. There are numerous advantageous aspects of the proposed converter. As an illustration, it employs a circuit consisting of an intercoupled inductor and a switched capacitor to amplify the voltage. This operates within a limited range of duty cycles, exerts minimal strain on the power electronics, and maintains a stable waveform for the input current. Moreover, in this design, the input and output ground are connected together. This study introduces an innovative design for high-voltage gain converters that are not isolated, with the goal of achieving a substantial improvement in voltage gain. This design integrates the dual boost converter with the layout of the switching inductor. The converter offers a wide range of duty cycle performance, a significant boost in output voltage, minimum stress on semiconductor devices, minimal losses during switching, and a high level of efficiency. It reduces voltage stress on all devices, ensures even distribution of current among inductors, and simplifies control, hence improving the stability of an inductor [16]. This converter is more compact, resulting in reduced dimensions and mass. In addition, the converter is able to work with a constant input current. The paper by [17] introduces a non-inverting transformerless step-up converter that achieves a significant increase in voltage. The converter integrates a constant input current, which simplifies the design of the input filter and enhances its longevity and reliability in various applications, including fuel cells. However, most step-up DC-DC converters that use coupled inductors see a significant rise in voltage across their active switch when it is switched off, mostly due to the presence of a leaky inductor. Consequently, the use of snubber circuits or a complex methodology is required. The study [18] introduces an improved DC-DC converter that utilizes a coupled inductor to achieve a quadratic increase in voltage. In order to accomplish this, we utilize an active clamp circuit that incorporates zero voltage switching (ZVS). This reduces the amount of heat transferred through conduction and makes it easier to achieve a high level of efficiency. This converter architecture has several benefits, such as a consistent input current, significant amplification, excellent efficiency, and a decreased component count compared to the output gain. An article published in [19] introduces a voltage converter with a substantial voltage boost. This converter utilizes switched capacitors and switched LCL (SLCL) cells as its core components. The proposed SLCL cell operates by employing a capacitor in place of the diode typically utilized in the conventional passive switched inductor cell. This results in an increase in voltage. The converter is configured to utilize two active switches, located at each terminal of the power supply, to both charge and discharge the cell inductors. The configuration of the converter normally consists of N cells in the terminals and M cells in the terminals, together with K SC cells. The recommended converter utilizes active switches that function at a conservative and reliable duty cycle of D = 0.51. This guarantees that the switches experience a voltage stress that is roughly 25% of the output voltage. The converter [20] operates with a reduced voltage across its capacitors in comparison to the voltage at the output port. This converter offers more voltage amplification than a conventional step-up converter. The modulation approach, known as the interleave scheme, reduces the voltage ripple in the output port and the input current, consequently improving the power quality. The converter effectively reduces voltage distortion in the output port without increasing the switching frequency or modifying the circuit parameters. In [21], the interleave technique is utilized to create a non-isolated converter that delivers a very high voltage gain. By minimizing conduction losses, the efficiency is enhanced. The clamp circuit is utilized to limit unwanted voltages and concurrently enhance the conversion factor of the proposed converter, leading to an amplified magnitude. The converter possesses notable characteristics such as reduced voltage stress on semiconductors, diminished diode reverse recovery,

decreased input current, minimal conduction losses, and elevated efficiency. Reference [22] proposes a more sophisticated setup of the positive output boost LUO converter. This circuit arrangement guarantees a consistent input current while also improving the ability to amplify voltage. The voltage boost technique has been utilized on two occasions, leading to a higher voltage amplification ratio in comparison to the initial method. The suggested architecture possesses several features, including a significant enhancement in voltage amplification when functioning with duty cycles lower than 50%. This work presents the development of a voltage multiplier cell-based quadratic boost converter that offers substantial voltage amplification. The converter is designed primarily for incorporation into renewable energy systems and can be used in any application that requires a high-efficiency, non-isolated converter. This converter has several advantages as follows:

- By employing a single switch, this research attains a substantial increase in output voltage gain, surpassing prior approaches that relied on several switches.
- The common ground denotes the mutual connecting point between the input and output ports.
- The voltage stress experienced by an active switch is often equal to ½ of the output voltage.
- Significant voltage gain.
- continuous input current.

2 The Structure of the Proposed Converter

The proposed converter aims to improve the voltage amplification of the second-order converter while maintaining its advantages. This system offers several advantages, including the precise alignment of the input and output ports, the capability to convert voltage while keeping the quadratic term of the duty cycle in the denominator, the inclusion of an input inductor, and the low distortion of the input current. To tackle these problems, a coupled inductor and a voltage multiplier circuit have been employed. Fig. 1 depicts the configuration of this converter. This converter includes an input inductor and a coupled inductor with two separate cores, five diodes, four capacitors, and an active switch. To examine the converter in steady state, we assume that the capacitors have a large enough capacity, resulting in a constant voltage at both ends. Similarly, the inductors are also assumed to have a high enough value, making the current passing through them constant. An ideal coupled inductor, along with diodes and an active switch, is considered in this converter. The converter has two operational states in one keying period, and Fig. 2 displays the key waveforms of the converter. In the remainder of this text, we will analyze each operational situation and provide the governing equations for each scenario.

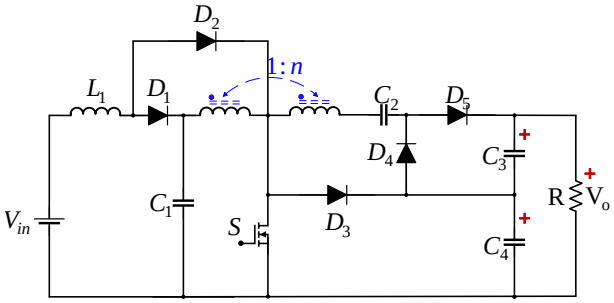

Fig. 1. Structure of the proposed converter

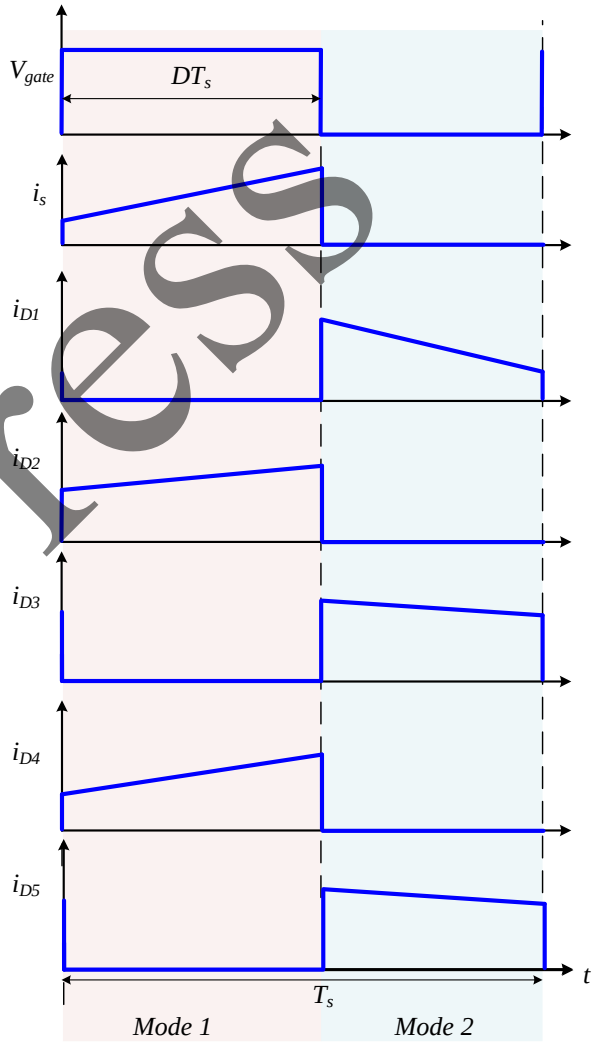

Fig. 2. Key waveforms of the proposed converter

In the first working situation, the gate is applied to the active switch of the converter. The L_1 gets charged through the V_{in} and charges C_1 and L_m. Diodes D_1, D_3, and D_5 remain reverse biased, while diodes D_2 and D_4 become forward biased. The equations that govern the converter in this situation are as follows:

$$v_{L_1} = V_{in} \quad (1)$$

$$v_{C_1} = v_{L_m} \quad (2)$$
$$v_O = v_{C_3} + v_{C_4} \quad (3)$$
$$v_{C_2} = nv_{C_1} + v_{C_4} \quad (4)$$
$$i_{C_1} = -(ni_{C_2} + i_{L_m}) \quad (5)$$
$$i_{C_3} = -i_O \quad (6)$$
$$i_{C_4} = -(i_O + i_{C_2}) \quad (7)$$

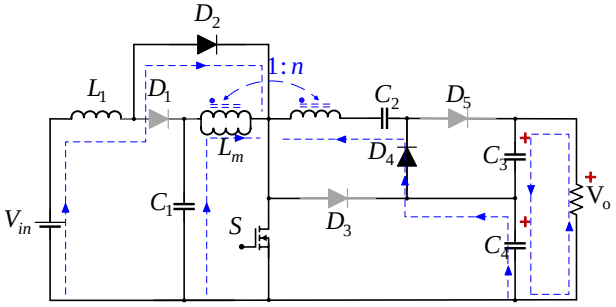

Fig. 3. The converter structure in the first working state.

In the second working state of the circuit, the gate signal is removed from the active switch, and the energy in $L_1$and L_m is transferred to the load. During this state, diodes D_1, D_3, and D_5 are forward biased, while diodes D_2 and D_4 are reverse biased. To begin a new working period, the gate signal is applied to the active switch (see Fig. 4). The equations governing the converter are provided below.

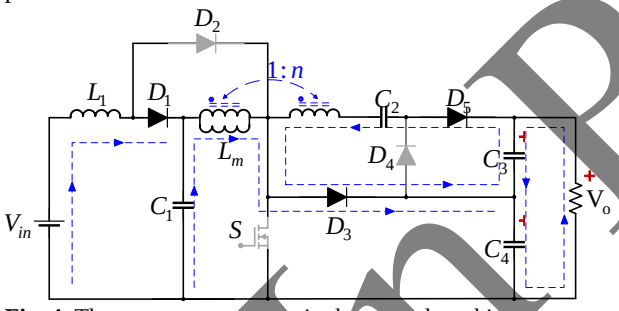

Fig. 4. The converter structure in the second working state.

$$v_{L_1} = V_{in} - v_{C_1} \quad (8)$$
$$v_{C_1} = v_{L_m} + v_4 \quad (9)$$
$$v_O = v_{C_3} + v_{C_4} \quad (10)$$
$$v_{C_2} = nv_{L_m} + v_{C_3} \quad (11)$$
$$i_{C_1} = i_{L_1} - i_{L_m} - i_{C_2} \quad (12)$$
$$i_{C_2} = -i_{C_3} - i_O \quad (13)$$
$$i_{C_4} = i_{C_3} + i_{L_m} - i_{C_2} \quad (14)$$

By applying the volt-second balance law to the $L_1$and L_m, we obtain the following equation.

$$\int_0^T v_{L_m(t)dt} = 0 \quad (15)$$
$$v_{L_m}^{off} = -\frac{dv_{C_1}}{1-d} \quad (16)$$
$$V_{C_4} = \frac{V_{C_1}}{1-d} \quad (17)$$
$$\int_0^T v_{L_1(t)dt} = 0 \quad (18)$$
$$V_{C_1} = \frac{V_{in}}{1-d} \quad (19)$$

By placing relation 12 in 17, the following relation is obtained.

$$V_{C_4} = \frac{V_{in}}{(1-d)^2} \quad (20)$$

By inserting (20) and (19) in (4), the voltage across C_2 is calculated as follows.

$$V_{C_2} = \frac{1 + n(1-d)V_{in}}{(1-d)^2} \quad (21)$$

By placing relations 16 and 21 in relation 11, the voltage of capacitor C_3 will be calculated as follows.

$$V_{C_3} = \frac{(1+n)V_{in}}{(1-d)^2} \quad (22)$$

By inserting formulas 22 and 20 in relation 3, the output voltage of the proposed converter will be calculated.

$$v_O = v_{C_3} + v_{C_4} = \frac{(2+n)V_{in}}{(1-d)^2} \quad (23)$$

Furthermore, the voltage gain of the suggested converter is determined using the following calculation.

$$\frac{V_O}{V_{in}} = \frac{(2+n)}{(1-d)^2} \quad (24)$$

A 3-D picture showing how the voltage gain varies with the coupled inductor's turn ratio and duty cycle may be found in Figure 5. Furthermore, Fig. 6 illustrates how the duty cycle and the coupled inductor turns ratio affect the voltage gain. Both figures allow you to analyze the impact of each variable on the voltage gain of the converter.

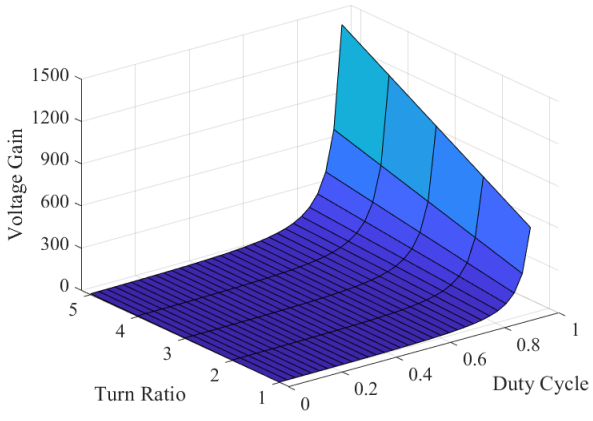

Fig. 5. 3-D display of voltage gains in terms of the coupled inductor's turn ratio and duty cycle.

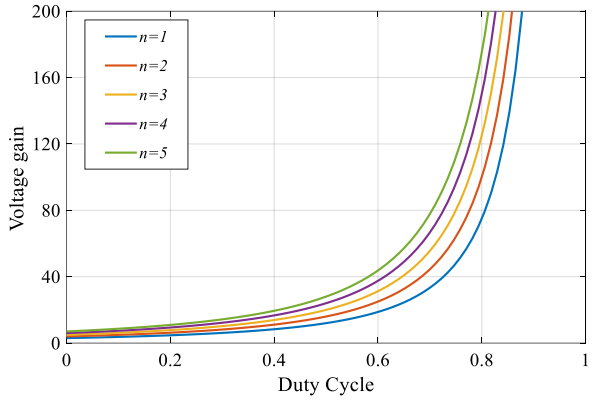

Fig. 6. Voltage gain as a function of duty cycle variations with the coupled inductor ratio

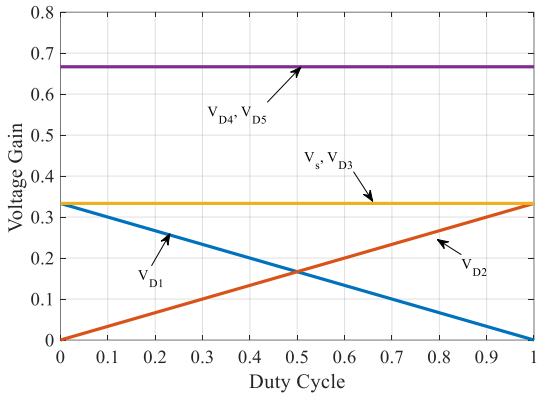

Fig. 7. Voltage stress diagram of semiconductor devices in terms of duty cycle changes and considering *n=1*

3 Voltage Stress on Semiconductor Devices

Equivalent circuits were used to calculate the maximum voltage applied to each semiconductor device in a steady state. If any of these devices disconnect, the maximum voltage of both ends will be applied. Diodes D_1, D_3, and D_5 in the first working state will have the highest voltage applied to them, since they are reversed-biased. Similarly, in the second working state, the active switch and diodes D_2, and D_4 are off, and the maximum voltage is applied at both ends. The proposed converter determines the reverse voltage applied to each semiconductor device based on specific relationships. Fig. 7 displays the voltage stress diagram of semiconductor devices, taking into account the changes in the duty cycle and assuming n=1. The voltage stress of the active switch remains constant at 1/3 of the output voltage, irrespective of any variations in the duty cycle. However, the voltage stress of D_1, and D_3 will exceed 1/3 of the output voltage. The voltage stress on the active switch and D_3 is shown in Fig. 8, whereas the voltage stress on D_1, and D_2 is shown in Fig. 9 and Fig. 10, respectively. Lastly, the voltage stress of D_4, and D_5 is shown in Fig. 11.

$$V_s = V_{D3} = -V_{C_4} = -\frac{V_{in}}{(1-d)^2} = -\frac{V_O}{2+n} \tag{25}$$

$$V_{D1} = -V_{C_1} = -\frac{V_{in}}{1-d} = -\frac{V_O(1-d)}{2+n} \tag{26}$$

$$V_{D2} = V_{C_1} - V_{C_4} = \frac{V_{in}}{1-d} - \frac{V_{in}}{(1-d)^2} = -\frac{dV_O}{2+n} \tag{27}$$

$$V_{D4} = V_{D5} = -V_{C_3} = -\frac{(1+n)V_{in}}{(1-d)^2} = -\frac{(1+n)V_O}{2+n} \tag{28}$$

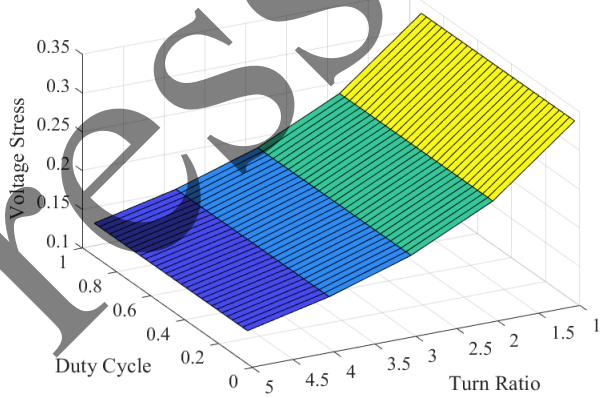

Fig. 8. 3-D voltage stress diagram for the diode D_3 based on variations in the coupled inductor's turns ratio and duty cycle.

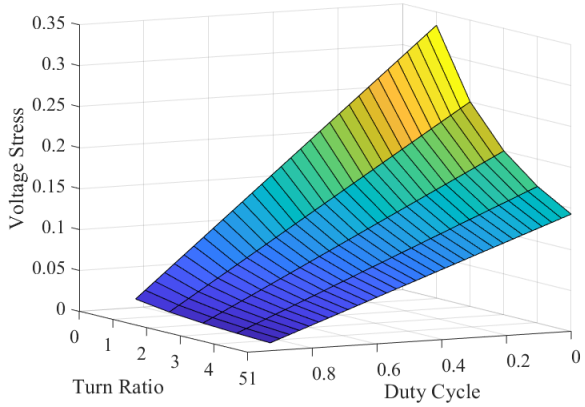

Fig. 9. 3-D voltage stress diagram for the diode D_1 based on variations in the coupled inductor's turns ratio and duty cycle.

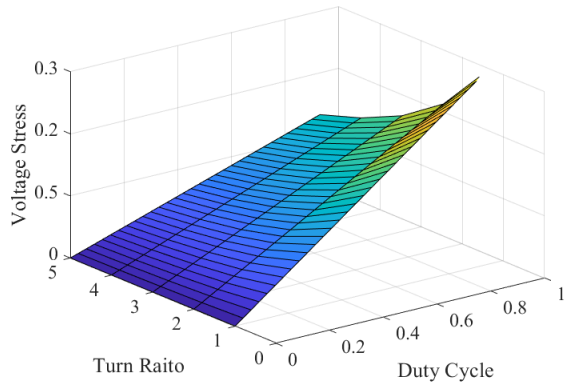

Fig. 10. 3-D voltage stress diagram for the diode D_2 based on variations in the coupled inductor's turns ratio and duty cycle.

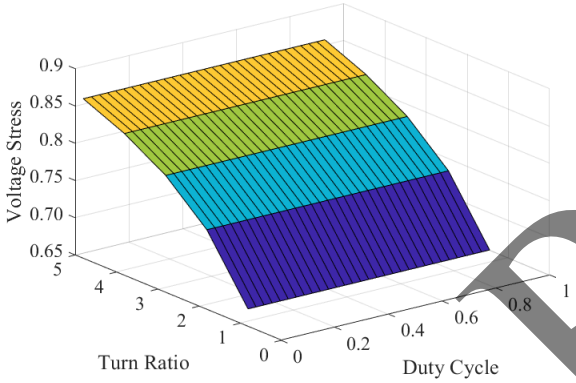

Fig. 11. 3-D voltage stress diagram for diodes D_4 and D_5 based on variations in the coupled inductor's turns ratio and duty cycle.

4 design

This section will calculate the relationship between the constituent values of the proposed converter. It will focus on the calculation of the sizes of inductors L_1 and L_m according to the first working condition.

$$v_{L_1} = L_1 \frac{\Delta i_{L_1}}{dT_s} \rightarrow L_1 = V_{in} \frac{d}{f_s \Delta i_{L_1}} \tag{29}$$

$$v_{L_m} = L_m \frac{\Delta i_{L_m}}{dT_s} \rightarrow L_m = V_{C_1} \frac{d}{f_s \Delta i_{L_m}} = \frac{V_O d(1-d)}{f_s \Delta i_{L_m}(2+n)} \tag{30}$$

The size of the converter capacitors is calculated using the charge stored in the capacitor in the first working state.

$$C_1 = \frac{(2+n)V_O d}{\Delta v_{C_1}(1-d)^2 R f_s} \tag{31}$$

$$C_2 = \frac{V_O d}{\Delta v_{C_2} R f_s} \tag{32}$$

$$C_3 = \frac{V_O d}{\Delta v_{C_3} R f_s} \tag{33}$$

$$C_4 = \frac{V_O d}{\Delta v_{C_4} R f_s} \tag{34}$$

5 Losses and efficiency

To convert electrical energy, some of it is lost as heat due to various factors. These include losses in the wiring or coils (known as winding or ohmic losses), losses in the magnetic core, and losses in the switches used to control the flow of electricity. However, using fast double diodes (called Schottky diodes) can help to reduce the losses associated with diodes. To calculate the amount of energy lost in the coils, we need to determine the amount of current passing through each coil.

$$i_{L_{1rms}} = \frac{2+n}{(1-d)^2} \frac{V_O}{R} \tag{35}$$

$$P_{WL_1} = \left(i_{L_{1rms}}\right)^2 r_{WL_1} = \left(\frac{2+n}{(1-d)^2} \frac{V_O}{R}\right)^2 r_{WL_1} \tag{36}$$

$$P_{copper} = R_1 I_{rms-N1}^2 + R_1 I_{rms-N2}^2 \tag{37}$$

$$I_{rms-Lm} = \sqrt{I_{Lm}^2 + \frac{\Delta I_{Lm}^2}{12}} \tag{38}$$

$$I_{rms-N1} = \sqrt{I_{rms-Lm}^2 + n I_{rms-N2}^2} \tag{39}$$

$$i_{L_{2rms}} = \frac{2+n+d^2}{d^2(1-d)^2} \tag{40}$$

Active switch losses are categorized into two types: conduction losses and switching losses. Each type of loss is calculated as follows.

$$P_{Switching-S} = P_{Sw.cond} + P_{Switching-S} \tag{41}$$

$$P_{Sw.cond} = i_{Sw.cond}^2 \times r_{Sw.ON} \tag{42}$$

$$I_{rms-Sw} = \frac{(2+n)\left(2-\sqrt{(1-d)}\right)}{d^2(1-d)^2} \frac{V_O}{R} \tag{43}$$

$$P_{Switching-S} = \frac{1}{2} C_S f_{sw} V_S^2 \tag{44}$$

6 Small signal analysis

In this section the small signal model of the proposed converter is carried out. The variables of steady state are $x = i_{L1}, i_{Lm}, V_{C1}, V_{C2}, V_{C3}, V_{C4}$. Assuming the input voltage and duty cycle as input vector "u", the output

capacitors voltage is selected as the output variable "*y*". The equation acquires via space vector linearization as follow:

$$\frac{d}{dt}\hat{\mathbf{x}} = \mathbf{A}\hat{\mathbf{x}} + \mathbf{B_1}\hat{d} + \mathbf{B_2}\hat{V}_{in} \quad (45)$$

$$\hat{y} = \mathbf{C}\hat{\mathbf{x}} + \boldsymbol{D}u \quad (46)$$

The dynamic equations are shown as below:

$$L_1\frac{di_{L1}}{dt} = dV_{in} + (1-d)(V_{in} - V_{C1}) \quad (47)$$

$$L_m\frac{di_{Lm}}{dt} = dV_{C1} + (1-d)(V_{C1} - V_{C4}) \quad (48)$$

$$C_1\frac{dV_{C1}}{dt} = -d\left(ni_{C_2} + i_{L_m}\right) + (1-d)(i_{L_1} - i_{L_m} - i_{C_2}) \quad (49)$$

$$C_2\frac{dV_{C2}}{dt} = -d\left(i_O + i_{C_4}\right) - (1-d)(i_O + i_{C_3}) \quad (50)$$

$$C_3\frac{dV_{C3}}{dt} = -di_O + (1-d)(\frac{i_O}{2}) \quad (51)$$

$$C_4\frac{dV_{C4}}{dt} = -d\left(i_O + i_{C_2}\right) + (1-d)(i_{C3} + i_{L_m} - i_{C_2}) \quad (52)$$

$$d = D + \hat{d} \quad (53)$$

The space vector matrices are derived by solving the above equations:

$$A = \begin{bmatrix} 0 & 0 & 1-d & 0 & 0 & 0 \\ 0 & 0 & 1 & 0 & 0 & 1-d \\ 1-d & 1 & 0 & 0 & 0 & 0 \\ 0 & d & 0 & 0 & 0 & 0 \\ 0 & 0 & 0 & 0 & 0 & 0 \\ 0 & 2d-1 & 0 & 0 & 0 & 0 \end{bmatrix} \quad (54)$$

$$B_1 = \begin{bmatrix} 0 \\ \frac{V_{C1}}{2L_m} \\ \frac{I_{L1}}{C_1} \\ \frac{I_{L2}}{C_2} \\ \frac{I_{L2}}{C_3} \\ \frac{I_{L2}}{C_4} \end{bmatrix} \quad (55)$$

$$B_2 = \begin{bmatrix} 1 \\ 0 \\ 0 \\ 0 \\ 0 \\ 0 \end{bmatrix} \quad (56)$$

$$C = [0 \quad 0 \quad 0 \quad 1 \quad 1 \quad 1] \quad (57)$$

$$D = \begin{bmatrix} 0 \\ 0 \end{bmatrix} \quad (58)$$

7 Simulation results

To conduct the simulation, we will first design the converter. To achieve this, we will calculate the size of each component of the converter based on the desired values mentioned in Table 1. We will use the design relationships mentioned in the previous chapter for this purpose. Table 2 provides the calculated values of the components of the converter based on relations 29 to 34.

Table 1. The desired values of the converter

parameters	size
Input voltage	24 V
Output voltage	230 V
Output power	120 W
Switching frequency	50 kHz
Δi_L	1 A
Δv_C	500 mV

Table 2 The designed values of the converter

parameters	size
L_m	377µH Core: EC36/21/11 Turn of winding = 12
L_1	211µH, Toroid core
C_1	100µF , 50V
C_2, C_3, C_3	10µF, 200 V
R_L	352Ω
Duty Cycle	44%
Active switch	IRFP250N
$D_1 - D_2 - D_3$	MBR10100
$D_4 - D_5$	MBR10200

In the circuit analysis, Fig. 12 shows the voltage of C_1. As per the calculation done in (19), the voltage of C_1 should be 43 volts, which matches voltage shown in Fig. 12. Additionally, Fig. 13 shows the voltage of 118 volts at both ends of capacitor C_2, which confirms (21_. Similarly, Fig. 14 represents the voltage across capacitor C_3. As per equation 22, the voltage value at both ends of capacitor C_3 should be 152.4 volts, which is shown in Fig. 14. Moreover, Fig. 15 represents the voltage across capacitor C_4, which is expected to be 77.5 volts as per relation 20. This figure confirms the same.

The voltage output of the proposed converter is depicted in Fig. 16. Relation 23 states that the output voltage of the proposed converter should be 230 volts, which is verified by Fig. 16.

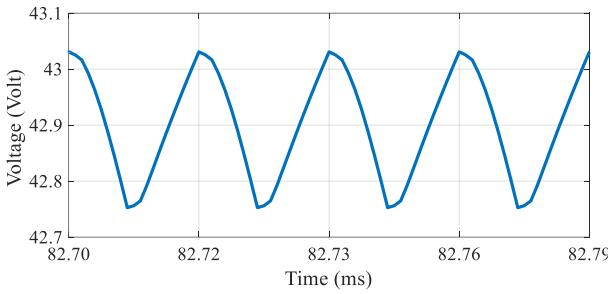

Fig. 12. Capacitor voltage C_1 of the proposed converter

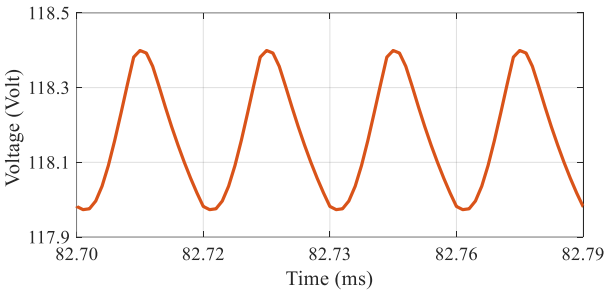

Fig. 13. Capacitor voltage C_2 of the proposed converter

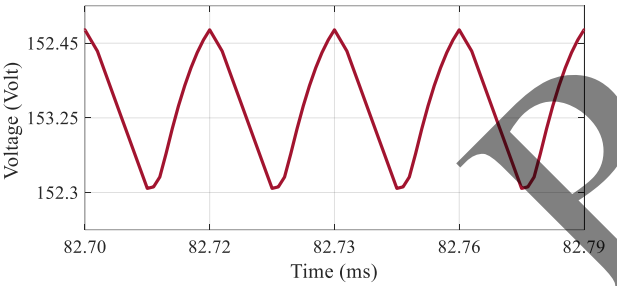

Fig. 14. Capacitor voltage C_3 of the proposed converter

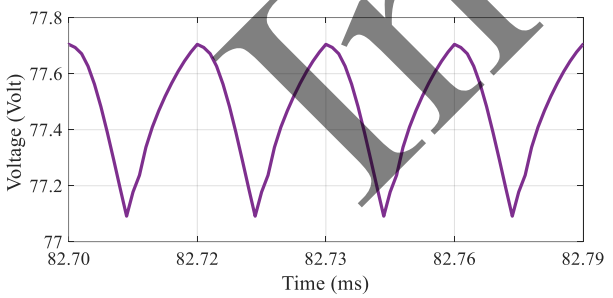

Fig. 15. Capacitor voltage C_4 of the proposed converter

Fig. 17 displays the voltage of D_1, which according to equation 25, should have a maximum reverse voltage of 42 volts. This value is confirmed in the figure. Similarly, Fig. 18 represents the voltage of diode D_2, which is applied with a voltage of 35 V in reverse mode. This value is also confirmed by (27). Furthermore, the maximum reverse voltage of diode D_3 and the active switch in the proposed converter has been calculated using (25). Lastly, according to relation 28, the maximum voltage of diodes D_4 and D_5 should be 150 volts, which is confirmed by Fig. 20 and Fig. 21.

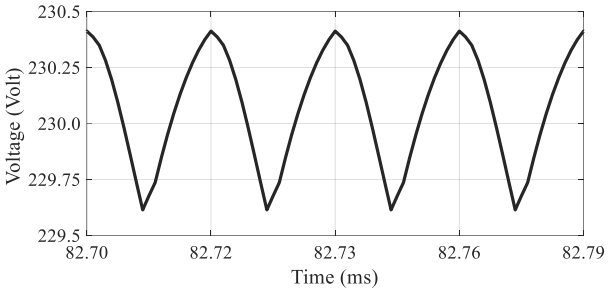

Fig. 16. Output voltage of the proposed converter

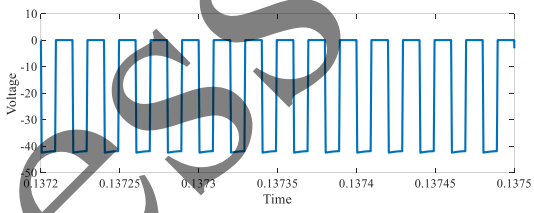

Fig. 17. Voltage across the diode D_1

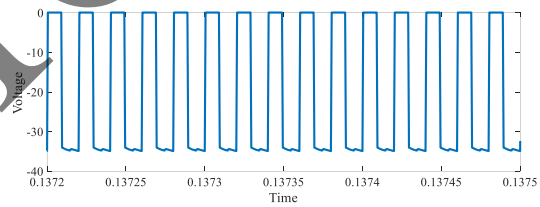

Fig. 18. Voltage across the diode D_2

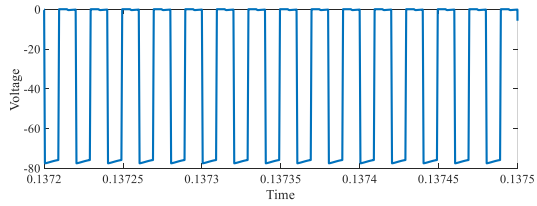

Fig. 19. Voltage across the diode D_3

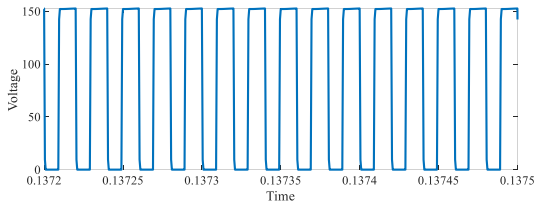

Fig. 20. Voltage across the diode D_4

Fig. 23 displays a current of 5 amps with 1-amp distortion in inductor L_1, given a converter power value of 120 watts.

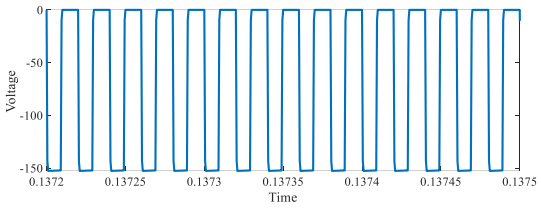

Fig. 21. Voltage across the diode D_5

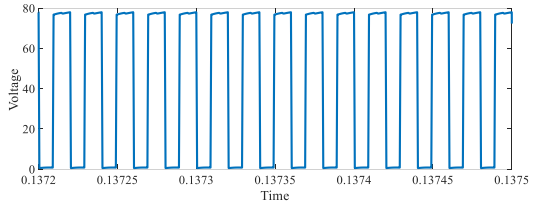

Fig. 22. Voltage across the active switch

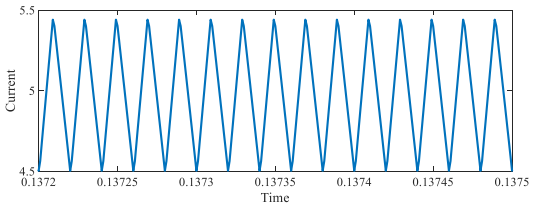

Fig. 23. input current (simulation result)

8 The results of the implementation of the laboratory sample

The proposed converter's calculated relationships reveal the components with appropriate nominal values for normal operation, as shown in Table 2. Fig. 24 shows the top view of the converter with all its components marked. The power section of the converter comprises power MOSFET (IRF250N), Schottky diodes (MBR 10100 and MBR10200), high-frequency inductors and capacitors. All capacitors used are of the electrolytic type, and the core of Guangzhou Tongyang Electronics brand is used to make the converter's inductor.

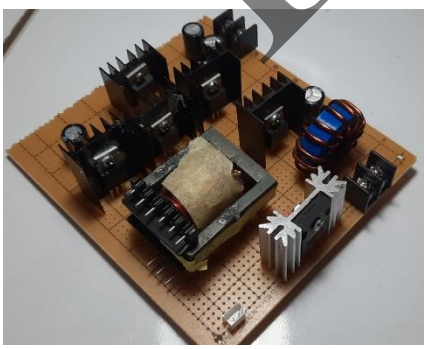

Fig. 24. Top view of the experimental version of the proposed converter

In Fig. 25 (a), the voltage across C_1 is displayed. As (19), the voltage of the capacitor should be 43 volts. The voltage of C_2 is shown in Fig. 25 (b), and the value of 115 volts confirms (21). Fig. 25 (c) shows the voltage of two ends of C_3, which has a value of 151 volts, confirming (22). The voltage across C_4 is displayed in Fig. 25 (d), and the value of 75 volts confirms (20). Finally, Fig. 26 displays the output voltage of the experimental sample, which has a value of 226 volts, confirming (23).

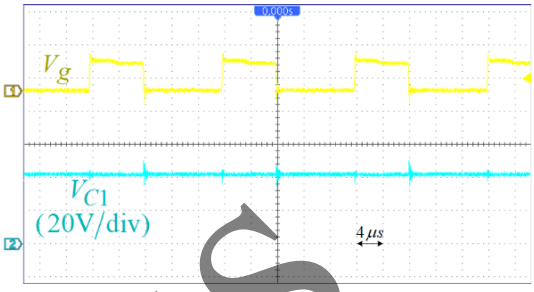

(a)

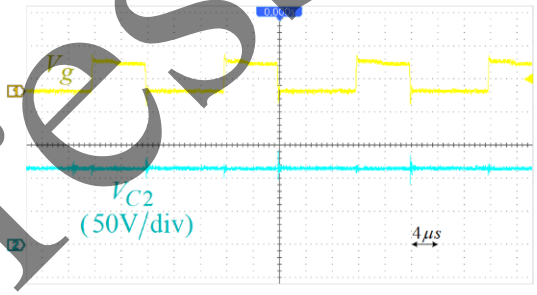

(b)

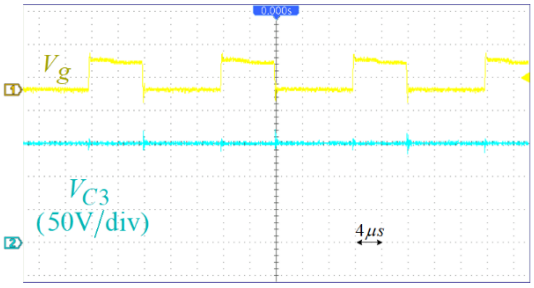

(c)

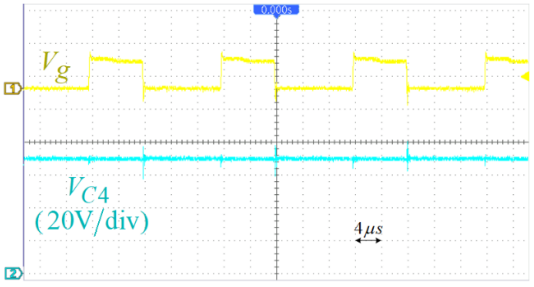

(d)

Fig. 25. Capacitors voltage (a) v_{c1}. (b) v_{c2}. (c) v_{c3}. (d) v_{c4}

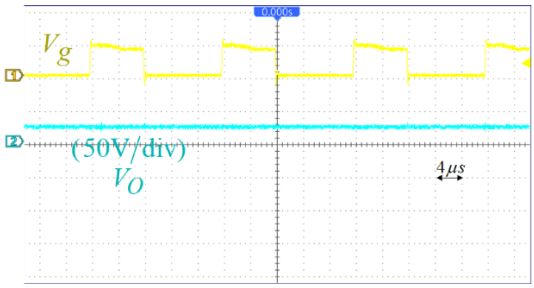

Fig. 26. Output voltage (experimental result)

The maximum reverse voltage of 42 volts is valid for diode D_1, as shown in Fig. 27 (a). Similarly, Fig. 27 (b) shows that the maximum voltage of 35 volts is valid for diode D_2 according to (27). Fig. 27 (c) displays the voltage across diode D_3, with a maximum voltage of 75 volts, which is valid based on (25). The voltage across diode D_4 is shown in Fig. 27 (d), and the maximum reverse voltage of 150 volts is valid according to (28). The voltage across diode D_5 is shown in Fig. 27 (e), and the maximum reverse voltage of 150 V is also valid according to equation 28. Fig. 27 (f) conclusively verifies that the maximum voltage of 75 volts is applicable to both terminals of the active switch, as stated in equation (25). The proper operation of the semiconductor devices in the converter is confirmed by analyzing the converter's switching frequency and working modes. Fig. 28 illustrates the effectiveness of the suggested converter. The highest attainable efficiency achievable using topology is 94.5%. The voltage output of a PV module usually ranges around 24 volts. Therefore, the proposed design can efficiently boost voltage in the range of 200-300W.

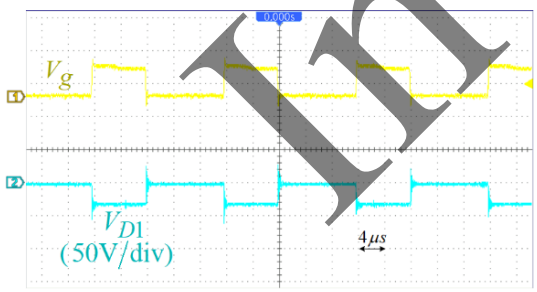

(a)

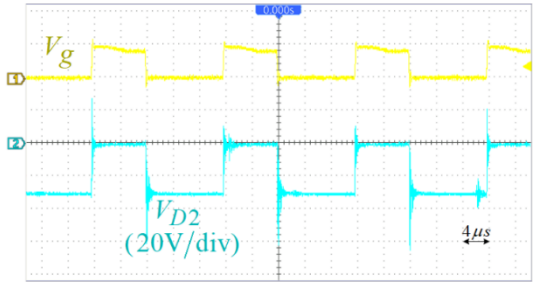

(b)

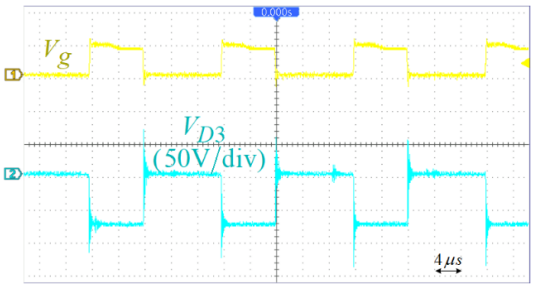

(c)

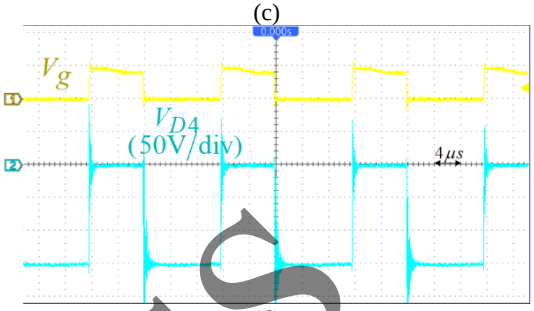

(d)

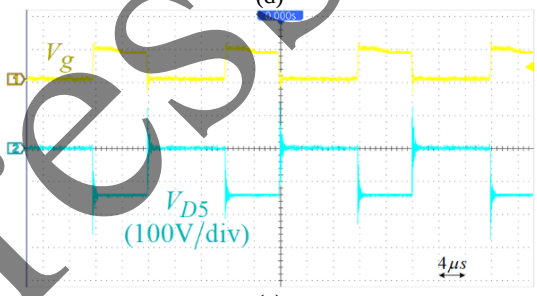

(e)

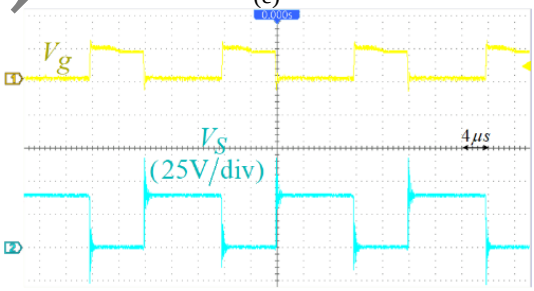

(f)

Fig. 27. The voltage across the semiconductor devices (a) V_{D1}. (b) V_{D2}. (c) V_{D3}. (d) V_{D4}. (e) V_{D5}. (f) V_S

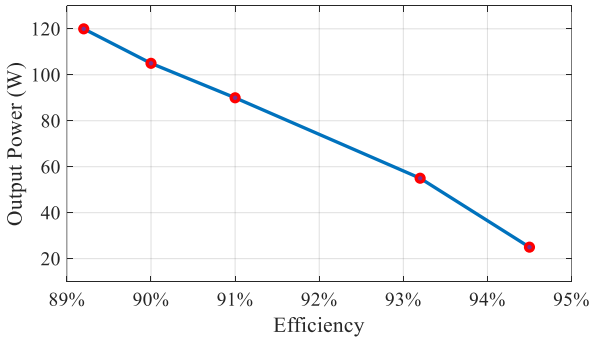

Fig. 28. The efficiency vs output power changes

9 Performance Comparison

This section compares and contrasts the suggested converter's performance with other converters mentioned in [12] and [13]. A study was undertaken to examine the performance of many aspects, such as voltage gain, active switch voltage stress, input current, the number of converter components, and common input and output ground. Fig. 29 depicts the correlation between the voltage gain of the converter and changes in the duty cycle, assuming *N=1*. Fig. 30 depicts the comparison of voltage stress on the active switch of the proposed converter with other similar converters. The converter [12] is the only converter, based on Fig. 30, that has a lower voltage stress than the suggested converter. Table 3 displays a comparison of the individual amounts of the proposed converter with other similar converters. Table 3 demonstrates that although the converter [12] may be more suitable in certain aspects, the control system of the converter becomes more costly and challenging due to the large number of components and the use of the interleave technique.

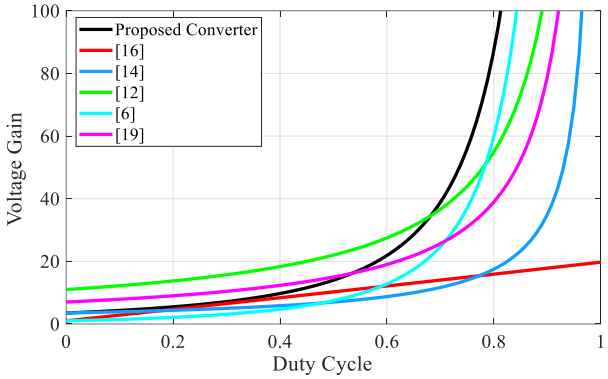

Fig. 29. The voltage gain point of view comparison between the suggested converter and comparable converters

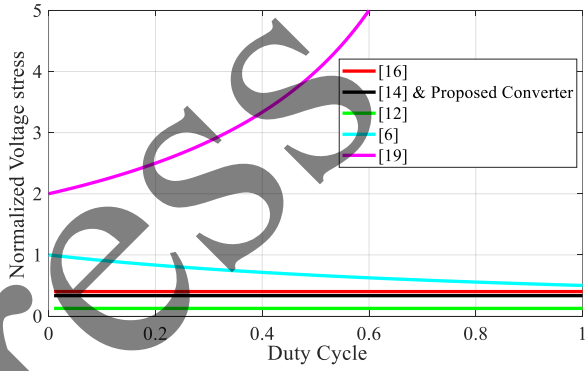

Fig. 30. The normalized voltage stress across the active switch compared between the suggested converter and a similar converter

Table 3 Comparative assessment of proposed topology with similar converters

Ref	Voltage gain	Voltage stress on active switch	S	L	C	D	Common ground	Continuous input current
Proposed Converter	$\frac{(2+n)}{(1-d)^2}$	$\frac{V_O}{2+n}$	1	2	4	5	Yes	Yes
[19]	$\frac{7+d}{1-d}$	$\frac{2}{1-d}$	2	4	5	7	No	Yes
[16]	$\frac{1+18.25d}{1-0.25d}$	$\frac{V_O}{2.5}$	2	4	2	8	No	Yes
[14]	$\frac{2+n_3}{(1-d)(1-n_2)}$	$\frac{1}{2+n_3}$	1	2	5	4	Yes	Yes
[12]	$\frac{6n+2}{1-d}$	$\frac{V_O}{2+6n}$	2	2	8	8	Yes	Yes
[6]	$\frac{1+d-2dn+nd+n^2d}{1-d}$	$\frac{V_O}{1+d+3dn+dn^2}$	1	2	3	2	No	Yes

10 Conclusion

This work proposes an enhanced high-gain, non-isolated quadratic step-up converter design that achieves a significant increase in voltage while operating at a shorter duty cycle. This makes it particularly well-suited for applications in distributed generation, such as solar power, as well as other fields. The proposed configuration simplifies the design by using fewer components, yet it still provides substantial quadratic voltage amplification. Typically, converters with quadratic voltage gain require more than three inductors and several diodes. Our continuous conduction mode (CCM) analysis incorporates comprehensive theoretical calculations to account for all losses generated by the converter's components. The voltage gain of this design has been validated through both theoretical calculations and experimental results, with a remarkable efficiency rating of 93.4% demonstrated in the initial version. Supporting this, simulation results obtained from SIMULINK software further substantiate our findings. Additionally, this study includes a comparative analysis of simulation and experimental outcomes. We also explore methods to mitigate the effects of parasitic resistances in passive components and switching, which can further enhance overall efficiency.

Conflict of Interest

The authors declare no conflict of interest.

Author Contributions

S. Hasanzadeh: Conceptualization, Methodology, Software, Formal analysis, Writing - Original draft, Supervision. **S. M. Salehi:** Revise & editing, Investigation. **M. J. Saadatmandfar:** Conceptualization, Methodology, Software, Formal analysis, Writing -Original draft.

Funding

No funding was received for this work.

Informed Consent Statement

Not applicable.

References

[1] H. Shojaeian, M. Heydari and S. Hasanzadeh, "Improved interleaved high step-up converter with high efficiency for renewable energy applications," *8th Power Electronics, Drive Systems & Technologies Conference (PEDSTC)*, Mashhad, Iran, 2017, pp. 288-293.

[2] Veerabhadra and S. Nagaraja Rao, "Assessment of high-gain quadratic boost converter with hybrid-based maximum power point tracking technique for solar photovoltaic systems," *Clean Energy*, vol. 6, no. 4, pp. 632–645, 2022.

[3] M. Forouzesh, Y. P. Siwakoti, S. A. Gorji, F. Blaabjerg, and B. Lehman, "Step-Up DC–DC Converters: A Comprehensive Review of Voltage-Boosting Techniques, Topologies, and Applications," *IEEE Trans. Power Electron*., vol. 32, no. 12, pp. 9143–9178, 2017.

[4] V. K. Goyal and A. Shukla, "Isolated DC–DC boost converter for wide input voltage range and wide load range applications," *IEEE Trans. Ind. Electron.*, vol. 68, no. 10, pp. 9527–9539, 2020.

[5] M. Shaabani, A. Mirzaei, M. Rezvanyvardom, F. Khosravi, and S. A. Gorji, "A Hybrid Switched-Inductor/Switched-Capacitor DC-DC Converter with High Voltage Gain Using a Single Switch for Photovoltaic Application," *Energies*, vol. 16, no. 14, p. 5524, 2023.

[6] P. Sarvghadi, A. Y. Varjani, and M. Shahparasti, "A high step-up transformerless DC–DC converter with new voltage multiplier cell topology and coupled inductor," *IEEE Transactions on Industrial Electronics*, vol. 69, no. 10, pp. 10162–10171, 2021.

[7] V. Abbasi, N. Talebi, M. Rezaie, A. Arzani, and F. Y. Moghadam, "Ultrahigh Step-Up DC-DC Converter Based on Two Boosting Stages with Low Voltage Stress on Its Switches," *IEEE Transactions on Industrial Electronics*, 2023.

[8] M. Rezaie and V. Abbasi, "Ultrahigh step-up DC–DC converter composed of two stages boost converter, coupled inductor, and multiplier cell," *IEEE Transactions on Industrial Electronics*, vol. 69, no. 6, pp. 5867–5878, 2021.

[9] H. S. Gohari, N. A. Mardakheh, H. Tarzamni, N. V. Kurdkandi, K. Abbaszadeh, and J. Kyyra, "Non-isolated Ultra-high Voltage Gain Coupled Inductor-based DC-DC Converter," *IEEE Transactions on Circuits and Systems II: Express Briefs*, 2023.

[10] S. M. Salehi, S. M. Dehghan and S. Hasanzadeh, "Ultra step-up DC-DC converter based on three windings coupled inductor," *7th Power Electronics and Drive Systems Technologies Conference (PEDSTC)*, Tehran, Iran, 2016, pp. 171-176.

[11] M. A. Vaghela and M. A. Mulla, "High Step-Up Gain Converter Based on Two-Phase Interleaved Coupled Inductor Without Right-Hand Plane Zero," *IEEE Trans Power Electron*, vol. 38, no. 5, pp. 5911–5927, 2023.

[12] S.-J. Chen, S.-P. Yang, C.-M. Huang, and P.-S. Huang, "Analysis and Design of a New High Voltage Gain Interleaved DC–DC Converter with Three-Winding Coupled Inductors for Renewable

Energy Systems," *Energies*, vol. 16, no. 9, p. 3958, 2023.
[13] M. Farsijani, S. Abbasian, H. Hafezi, and A. Abrishamifar, "A high step-up cost-effective DC-to-DC topology based on three-winding coupled-inductor," *IEEE Journal of Emerging and Selected Topics in Industrial Electronics*, vol. 4, no. 1, pp. 50–59, 2022.
[14] T. Jin, X. Yan, H. Li, J. Lin, Y. Weng and Y. Zhang, "A New Three-Winding Coupled Inductor High Step-Up DC–DC Converter Integrating With Switched-Capacitor Technique," *IEEE Transactions on Power Electronics*, vol. 38, no. 11, pp. 14236-14248, Nov. 2023.
[15] A. Samadian, M. G. Marangalu, H. Tarzamni, S. H. Hosseini, M. Sabahi, and A. Mehrizi-Sani, "High Step-Up Common Grounded Switched Quasi Z-Source DC–DC Converter Using Coupled Inductor with Small Signal Analysis," *IEEE Access*, vol. 11, pp. 120516–120529, 2023.
[16] A. S. Mansour, A.-H. H. Amer, E. E. El-Kholy, and M. S. Zaky, "High gain DC/DC converter with continuous input current for renewable energy applications," *Scientific Reports*, vol. 12, no. 1, p. 12138, 2022.
[17] A. H. Mahdizadeh, M. Kashani, M. Soltani, A. Hajizadeh and S. A. Gorji, "A Quadratic Boost Converter Suitable for Fuel Cell-Powered Electric Vehicles," *IECON 2023- 49th Annual Conference of the IEEE Industrial Electronics Society*, Singapore, Singapore, 2023, pp. 1-6.
[18] M. Izadi, A. Mosallanejad, and A. Lahooti Eshkevari, "An improved coupled inductor-based quadratic step-up DC–DC converter with a high step-up factor and reduced voltage overshoot on the power switch," *IET Power Electronics*, 2023.
[19] N. Tewari, N. Paul, M. Jayaraman, and M. Prabhakar, "Reconfigurable high step-up DC to DC converter for microgrid applications," *IET Power Electronics*, 2023.
[20] J. C. Hernandez-Ochoa, A. Alejo-Reyes, J. C. Rosas-Caro, and J. E. Valdez-Resendiz, "Improved Operation of the Step-Up Converter with Large Voltage Gain and Low Voltage on Capacitors," *Applied Sciences*, vol. 13, no. 5, p. 2854, 2023.
[21] R. Fani and N. Erfani Majd, "Interleaved converter with ultra-high voltage gain for DC microgrid application," *International Journal of Electronics*, pp. 1–20, 2023.
[22] S. A. Gorji and H. Gholizadeh, "A Modified Positive Output Super-Lift Luo DC-DC Converter with Improved Voltage Boost Ability," in *2022 5th International Conference on Renewable Energy and Power Engineering (REPE)*, IEEE, 2022, pp. 282–286.

Saeed Hasanzadeh was born in Shirvan, Iran, in 1981. He received his B.Sc. degree in electrical engineering from Shahroud University of Technology, Shahroud, Iran, in 2003. He then went on to earn his MSc. and Ph.D. degrees in electrical engineering from the University of Tehran (UT), Tehran, Iran, in 2006 and 2012, respectively. His MSc thesis focused on High Voltage Engineering, while his Ph.D. dissertation was in the field of Wireless Power Transfer (WPT). In 2013, Dr. Hasanzadeh joined the Department of Electrical and Computer Engineering at Qom University of Technology as an Assistant Professor. Since 2022, he has been promoted to the position of Associate Professor. He is currently serving as the Dean of the Department of Electrical and Computer Engineering (ECE) at the same university since 2018. Dr. Hasanzadeh is an editorial board member of the Power Electronics Society of Iran (PELSI) and a Technical Program Committee (TPC) member of the IEEE Power Electronics & Drives: Systems and Technologies Conference (PEDSTC). He was the recipient of the Top Research Prize of Qom University of Technology in 2019 and 2023 and was recognized as an Outstanding Lecturer at the same university in 2020 and 2022. In 2023, he was elected as the top innovator of Qom province for presenting two innovative products in the field of partial discharge detection. His current research interests include power electronics, electrical machines, wireless power transfer, and high voltage engineering.

Seyed Mohsen Salehi received his B.Sc. degree from Shahab Danesh University, Qom, Iran, in 2012 and his M.Sc. degree from Qom University of Technology, Qom, in 2016, both in the field of electrical engineering. His research interests focus on the design, modeling, and control of power electronics converters, as well as their applications in electrical traction systems.

Mohammad Javad Saadatmandfar received his B.Sc. degree from Shahab Danesh University, Qom, Iran, in 2011 and his M.Sc. degree from Qom University of Technology, Qom, in 2024, both in the field of electrical engineering. His research interests focus on the design, modeling, and control of power electronics converters, as well as their applications in electrical power systems.